Scientific
Research
Publishing

Modeling and Numerical Simulation of Material Science

9 772164 534004   04

https://www.scirp.org/journal/mnsms

Journal Editorial Board

Table of Contents

Volume 13   Number 4   **October 2023**

Modeling and Numerical Simulation of Material Science (MNSMS)
Journal Information

COPYRIGHT

Comparative Performance Analysis of MAPbI₃ and FAPbI₃ Perovskites: Study of Optoelectronic Properties and Stability

Idrissa Diomandé[1,2*], Amal Bouich[1], Aka Aka Hyacinthe[1,2], Bernabe Mari Soucasse[1], Aka Boko[2]

[1]Institut de Disseny i Fabricació, Universitat Politècnica de València, Valence, Spain
[2]Laboratoire des Sciences Fondamentales et Appliquées (SFA), Université Nangui Abrogoua (UNA), Abidjan, Côte d'Ivoire
Email: *idiomande13@yahoo.fr

Abstract

The exploitation of fossil resources to meet humanity's energy needs is the root cause of the climate warming phenomenon facing the planet. In this context, non-carbon-based energies, such as photovoltaic energy, are identified as crucial solutions. Organic perovskites MAPbI₃ and FAPbI₃, characterized by their abundance, low cost, and ease of synthesis, are emerging as candidates for study to enhance their competitiveness. It is within this framework that this article presents a comparative analysis of the performances of MAPbI₃ and FAPbI₃ perovskites in the context of photovoltaic devices. The analysis focuses on the optoelectronic characteristics and stability of these high-potential materials. The optical properties of perovskites are rigorously evaluated, including band gaps, photoluminescence, and light absorption, using UV-Vis spectroscopy and photoluminescence techniques. The crystal structure is characterized by X-ray diffraction, while film morphology is examined through scanning electron microscopy. The results reveal significant variations between the two types of perovskites, directly impacting the performance of resulting solar devices. Simultaneously, the stability of perovskites is subjected to a thorough study, exposing the materials to various environmental conditions, highlighting key determinants of their durability. Films of MAPbI₃ and FAPbI₃ demonstrate distinct differences in terms of topography, optical performance, and stability. Research has unveiled that planar perovskite solar cells based on FAPbI₃ offer higher photoelectric conversion efficiency, surpassing their MAPbI₃-based counterparts in terms of performance. These advancements aim to overcome stability constraints and enhance the long-term durability of perovskites, ultimately aiming for practical application of these materials. This comprehensive comparative analysis provides an enlightened understanding of the optoelectronic performance and stability of MAPbI₃ and FAPbI₃ perovskites, which is critically important to

guide future research and development of solar devices that are both more efficient and sustainable.

Keywords

Perovskites, FAPbI$_3$, MAPbI$_3$, Optoelectronic Properties, Performance

1. Introduction

In recent years, tremendous progress has been made in the field of perovskite-based solar cells [1]. Perovskites are crystalline compounds with an ABX$_3$ chemical structure, where A represents a monovalent cation, B represents a divalent cation, and X represents a halide anion [2]. Within just a decade, their conversion efficiencies have increased from 6% to 25% [3]. The ongoing investigations regarding these materials aim to achieve a yield rate of 30% in the coming years [4]. These advancements are attributed to the multiple advantages offered by perovskites, including their broad optical absorption [5], making them promising candidates for solar energy harvesting [6]. Furthermore, perovskites stand out due to their ease of synthesis from abundant and low-cost materials [7], paving the way for large-scale production. Among the various perovskite variants, MAPbI$_3$ (methylammonium lead triiodide) and FAPbI$_3$ (formamidinium lead triiodide) compounds have demonstrated particularly promising properties for photovoltaic applications [8]. So far, the methylammonium (MA) cation has been the most studied, but MA-based perovskites generally exhibit band gaps greater than 1.55 eV [9], limiting their optical absorption range and photoelectrical conversion efficiency [10]. To address this issue, the formamidinium (FA) cation has been developed as a more efficient absorber, with a narrower band gap of 1.47 eV [11] compared to MAPbI$_3$. Current research focuses on improving the stability of these materials to make them more suitable for large-scale utilization [12]. Materials and processes have been developed to address this challenge, and the use of FA as a replacement for MA has contributed to reducing the band gap towards a more ideal range [13]. Additionally, hybrid organic/inorganic perovskites have been explored, featuring high absorption coefficients, appropriate band gaps, and long carrier lifetimes with high mobility [14] [15]. Another crucial aspect is enhancing the stability of perovskites as it represents a major hurdle for their long-term utilization [16]. In this regard, a comprehensive comparative analysis of the optoelectronic performance and stability of MAPbI$_3$ and FAPbI$_3$ perovskites has been conducted. This analysis encompassed several key aspects such as the optical properties of perovskites, the crystal structure of perovskite films characterized by X-ray diffraction (XRD), the film morphology analyzed using scanning electron microscopy (SEM). The main objective was to identify significant differences between MAPbI$_3$ and FAPbI$_3$ in terms of optoelectronic performance and stability and determine the key factors influencing the durability of these materials. Additionally, resistivity and conductivity measurements

were performed on the films. The obtained results demonstrated good crystallinity as well as higher efficiency and stability of the FAPbI$_3$ film compared to the MAPbI$_3$ film. These findings will provide valuable insights to guide research and development of novel strategies to enhance the efficiency and stability of perovskite-based solar cells.

2. Materials and Experimental Procedure

2.1. Materials

The necessary reagents for the synthesis of MAPbI$_3$ and FAPbI$_3$ perovskites were purchased from Sigma Aldrich, St. Louis, MO, USA, without requiring prior purification. The films were synthesized using perovskite solutions prepared from the following precursors: methylammonium iodide (MAI) with a concentration of 99.99%, formamidinium iodide (FAI) with a concentration of 99.99%, and lead (II) iodide (PbI$_2$) with a concentration of 99.99%. The preparation of perovskite solutions was carried out in small, very dark brown glass vials to prevent any undesirable reaction with light. For the preparation of FAPbI$_3$, the PbI$_2$ and FAI precursors were dissolved in a solvent mixture consisting of 90% anhydrous N,N-dimethylformamide (DMF) and 10% dimethyl sulfoxide (DMSO). As for the preparation of MAPbI$_3$, the PbI$_2$ and MAI precursors were dissolved in the same solvent mixture. Chlorobenzene (or toluene) was used as an antisolvent during the deposition of the perovskite films.

2.2. Production of the Films

Perovskite films were fabricated on pre-cleaned FTO glass substrates. The substrates were washed with Hell Max soap solution in distilled water, followed by rinsing with ethanol and acetone using an ultrasonic bath. Subsequently, any residual organic matter was removed through UV-Ozone treatment. To prepare PbI$_2$ solutions, 0.461 g of PbI$_2$ was dissolved in 1 ml of a solvent mixture consisting of 90% DMF and 10% DMSO. This dissolution was carried out in a small dark brown bottle. The resulting solutions were heated at 60˚C for two hours on a hot plate. To obtain perovskite solutions, each bottle containing MAI and FAI received 1 ml of PbI$_2$ solution. The obtained solutions were heated at 60˚C for two hours. For deposition, a volume of 100 µL of perovskite solution was used to coat the FTO glass substrate through centrifugation at a speed of 4000 revolutions per minute for 20 seconds using a spin-coater. The thickness of the deposited thin film depended on the spin-coater rotation time [17]. During this process, a few drops of chlorobenzene or toluene were deposited on the still wet perovskite films. Finally, the obtained deposits underwent thermal annealing. MAPbI$_3$ was annealed at 150˚C [18] for 20 minutes on a hot plate, while FAPbI$_3$ was annealed at 200˚C [19] for 20 minutes on a hot plate as shown in Figure 1.

2.3. Lattice Parameters

The parameters were calculated using the following equations:
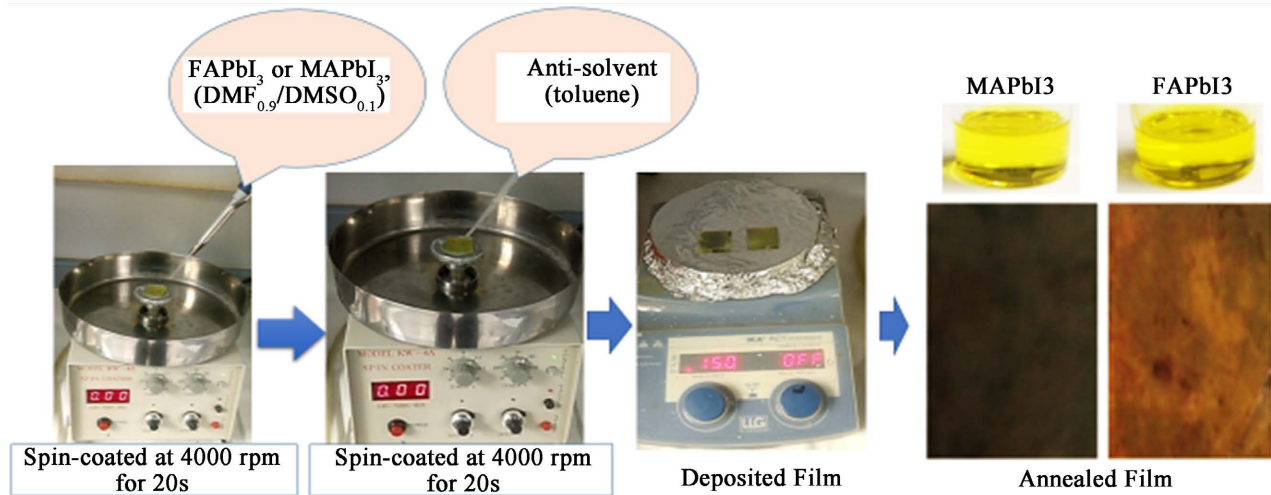
Figure 1. FAPbI₃ and MAPbI₃ Perovskites films synthesis procedures and sample photographs.

$$\frac{1}{d^2} = \frac{h^2 + k^2}{a^2} + \frac{l^2}{c^2} \tag{1}$$

$$\text{and} \quad n\lambda = d\, 2\sin(\theta) \tag{2}$$

2θ: Diffraction angle of the corresponding plane.

λ: Wavelength of the CuK α radiation (0.154 nm),

h, k, l: Miller indices and a and c are lattice constants, d: Inter-planar-spacing,

a, c: Lattice constants,

Octahedral factor

In the ABX₃ frame work perovskites, the stability of the BX₃ octahedron is predicted by the octahedral factor: μ

$$\mu = \frac{r_B}{r_X} \quad \text{Or} \quad \mu_n = \frac{\sum_{i=1}^{n} r_{B^i}}{\sum_{i=1}^{n} r_{X^i}} \tag{3}$$

If $0.41 < \mu < 0.73$, the coordination is octahedral.

Goldschmidt tolerance factor

The Goldschmidt tolerance factor t is established by the relationship [20]:

$$t = \frac{r_A + r_X}{\sqrt{2}\left(r_B + r_X\right)} \quad \text{Or} \quad t = \frac{\sum_{i=1}^{n}\left(r_{A^i} + r_{X^i}\right)}{\sqrt{2}\sum_{i=1}^{n}\left(r_{B^i} + r_{X^i}\right)} \tag{4}$$

you < 0.75 ilmènite	0.75 < t < 1.06 pérovskite			you > 1.06 hexagonal
	0.75 < t < 0.95 Orthorhombic distortion	0.96 < t < 0.99 Rhombohedral distortion	0.99 < t < 1.06 Cubic	

Grain size and effective lattice strain

The calculation of the effective grating deformation gives an overview of the defects and distortions of the grains at the level of the films, for the calculation we use the equation:

$$\cos\theta\beta_r = 4\varepsilon\sin\theta + \frac{k\lambda}{D} \tag{5}$$

k: Constant whose value is 0.94, λ: 0.15406 nm wavelength of the X ray source, D: Crystallite size or half-width (FWHM), ε: Deformation, θ: Position of the peak in radians where is the Bragg angle.

Dislocation density

The dislocation density of the crystal was evaluated using the formula;

$$\gamma = \frac{1}{D^2} \tag{6}$$

Absorption coefficient

Perovskites are direct band gap semiconductors. The energy band gap is calculated from an estimate of the trace $(\alpha h\nu)^2$ with respect to $h\nu$.

$$(\alpha h\nu)^2 = B(h\nu - Eg) \tag{7}$$

$$\alpha = \frac{1}{t}\ln\left(\frac{1}{T}\right) \tag{8}$$

α: Absorption coefficient,
h: Planck constant,
Eg: Forbidden band energy,
t: Thickness of the layers,
B: Constant.

Degradation rate (D)

$$D = \frac{A_\circ - A}{A_\circ} \tag{9}$$

or $A_\circ$ absorption of fresh sample A old sample absorption

3. Results and Discussions

Figure 2 shows the curves of the octahedral factor (μ) and the Goldschmidt tolerance factor (t). The calculated octahedral factors have a constant value of 0.4454 (**Table 1**), which corresponds to a range of values of $0.41 < \mu < 0.73$. According to Pauling's rules for cation/anion geometry, this indicates octahedral coordination [21] [22]. The calculated values of the Goldschmidt tolerance factors are listed in **Table 1**. The t factor for FAPbI$_3$ (1.0517) is significantly higher than that of MAPbI$_3$ (0.9717). However, the calculated values of the Goldschmidt tolerance factors range between 0.813 and 1.107, confirming the formation of halide perovskites [23] [24].

Figure 3 shows XRD diffraction spectra of MAPbI$_3$ and FAPbI$_3$ films. In the MAPbI$_3$ spectrum, the 2θ value of 12.80° represents unreacted residual PbI$_2$ [25]. The corresponding peak for FTO is located around 37.83° [26]. Characteristic peaks in the MAPbI$_3$ spectrum are found at 2θ coordinates of 14.24° and 28.57°, corresponding to the planar orientations of (110) and (220) that represent parallel planes in the perovskite structure [27]. These peaks indicate preferential growth of this layer in the tetragonal direction [28]. Both of these characteristic

Table 1. Values of the octahedral factor (μ) and the Goldschmidt tolerance factor (t) for the perovskites FAPbI₃ and MAPbI₃.

	FAPbI₃	MAPbI₃
t	1.0517	0.9717
μ	0.44545	0.44545
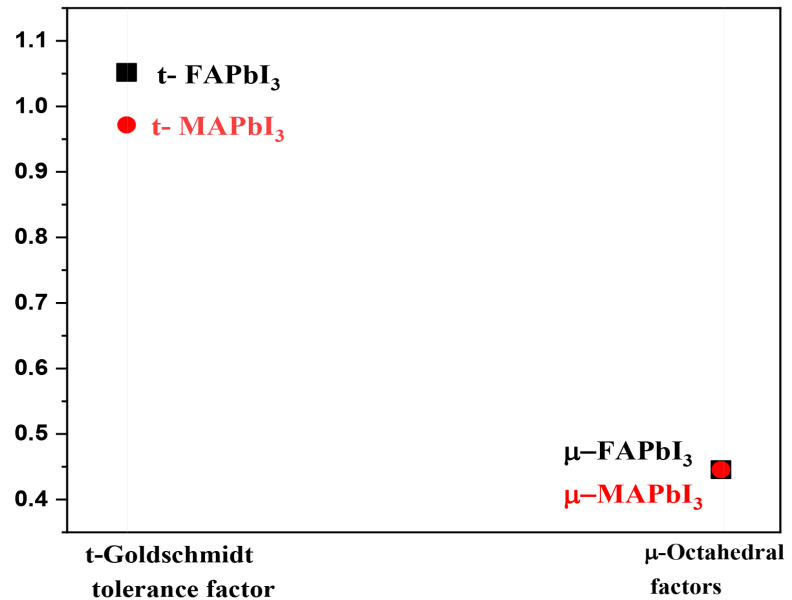
Figure 2. patterns of Goldschmidt and octahedral factors of FAPbI₃ and MAPbI₃ Perovskites films.
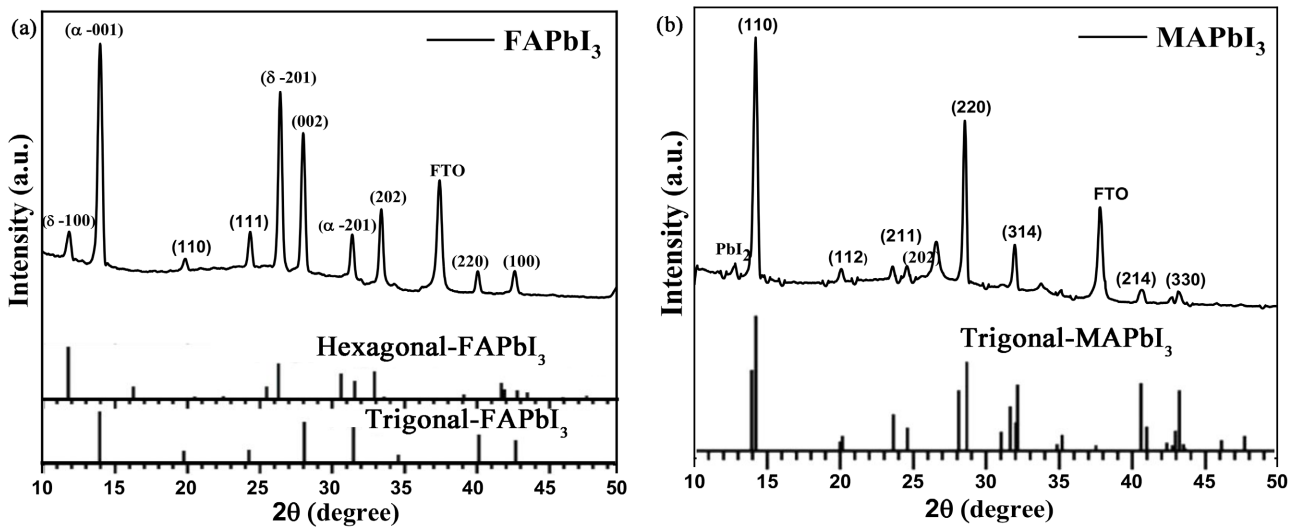
Figure 3. XRD patterns of FAPbI₃. (a) MAPbI₃; (b) Perovskites films.

peaks have higher intensities compared to the other peaks. Similarly, medium intensity peaks are observed at positions 20.17˚, 23.83˚, 24.73˚, 31.54˚, 40.74˚, and 43.74˚, corresponding to the planar orientations of (112), (211), (202), (314), (214), and (330). These peaks coincide with the reference peaks [29]. In the

FAPbI$_3$ spectrum, there are the desired alpha (a) phase and the gamma (δ) phase. The characteristic peak intensities for the alpha (a)-FAPbI$_3$ phases are located at positions 14.06° and 28.17°, corresponding to the (001) and (002) orientations, which are parallel planes within the structure. For the same alpha (a)-FAPbI$_3$ phase, peaks are observed at 20.07°, 24.10°, 28.17°, 31.95°, 40.28°, and 42.78°, which correspond to the (110), (111), (002), (202), (202), and (100) orientations. These peaks coincide with the reference peaks [30]. The gamma (δ)-FAPbI$_3$ phase exhibits peaks at 2θ values of 11.34° (001), 25.93° (201), and 32.53° (202). It can be observed that FAPbI$_3$ undergoes nearly complete conversion, with distinct peaks that match the reference peaks and almost no residual PbI$_2$ peaks.

The data in the Table 2 allows us to plot the curves of the FWHM, D the grain size, d the interplanar spacing, the γ dislocation density and the ε deformation: Figure 4.

The FWHM data represents the (110) and (220) peaks of FAPbI$_3$ and MAPbI$_3$ perovskites. Around the 14.0° peak, the FWHM value of MAPbI$_3$ is higher than that of FAPbI$_3$, while around the 28° peak, the FWHM value of FAPbI$_3$ is higher than that of MAPbI$_3$. Structural parameters were calculated using the Williamson-Hall (WH) plot method in Table 2 based on XRD analysis data. The interplanar spacing (d) value of FAPbI$_3$ is larger than that of MAPbI$_3$. Similarly, the grain size of FAPbI$_3$ is larger than that of MAPbI$_3$. Moreover, the average dislocation density (γ) and strain (ε) values are higher for FAPbI$_3$ compared to MAPbI$_3$. XRD analysis of the data reveals significant differences between FAPbI$_3$ and MAPbI$_3$.

The SEM images shown in Figure 5(a) & Figure 5(b) display the FAPbI$_3$ film (a) and the MAPbI$_3$ film (b). It can be observed that they have good adhesion to the substrate and are relatively rough. The surface roughness is correlated with the presence of grains, and we note that the surface of the FAPbI$_3$ film is rougher with more pores compared to the MAPbI$_3$ film. The multiplicity of pores and surface roughness allow the films to trap more light [31] [32].

Optical properties

The analysis of optical properties of thin perovskite films was conducted in

Table 2. Values of the parameters of the angle 2θ, FWHM, d inter-planar-spacing; D grain size, γ Dislocation density and ε strain for peaks (110) and (220).

Material	h, k, l	2θ (degree)	FWHM (m)	d (nm)	D (nm)	$\gamma\, 10^{-3}$ (nm^{-2})	$\varepsilon\, 10^{-3}$
MAPbI$_3$	110	14.24	0.30	6.21	26.51	1.42	10.55
	220	28.57	0.18	3.12	44.55	0.50	3.15
	Medium			4.67	35.53	0.96	6.85
FAPbI$_3$	001	14.06	0.29	6.30	29.13	1.36	10.44
	002	28.17	0.20	3.16	48.55	0.61	3.51
	Medium			4.73	38.84	0.98	6.97
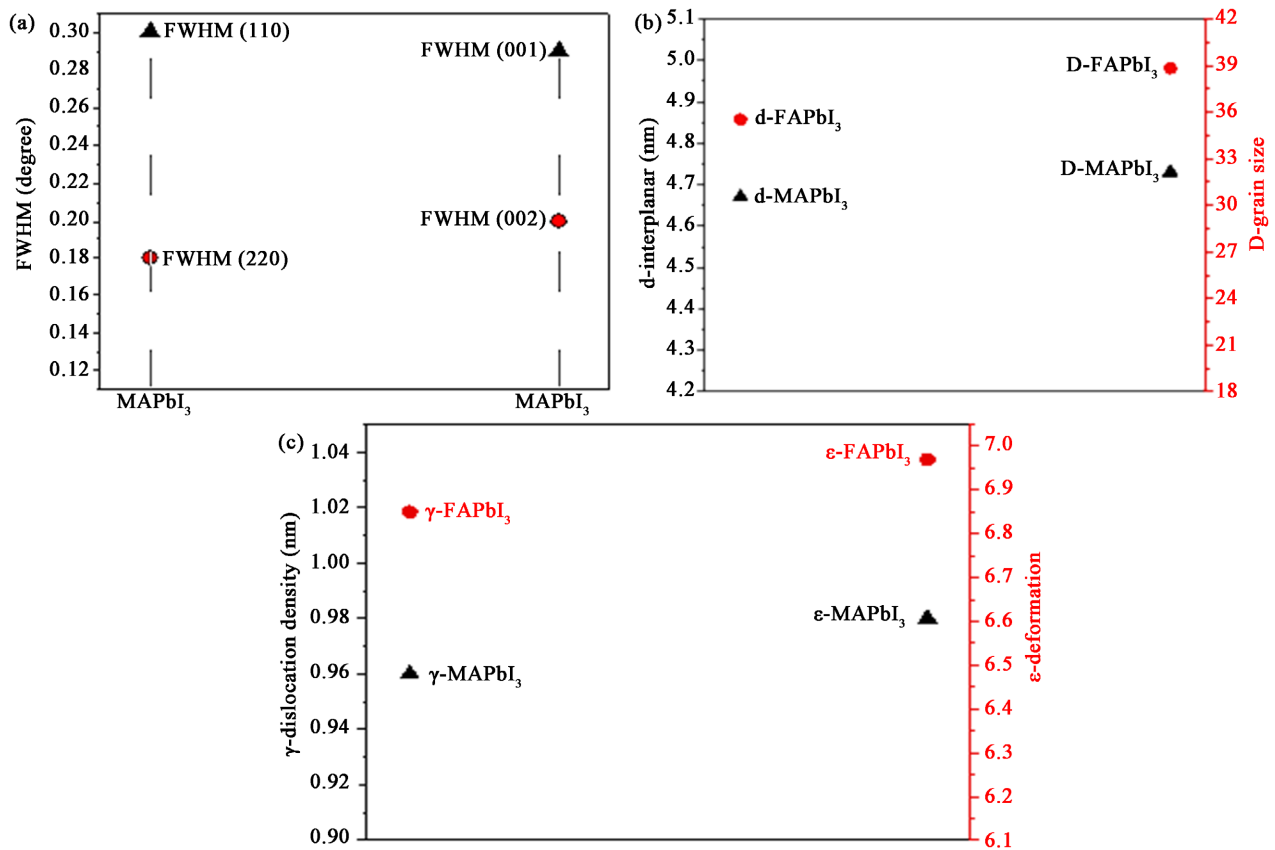
Figure 4. (a) FWHM of (110) and (220), (b) *D*-grain size and *d*-interplanar spacing peaks (110) and (220) and (c) *γ*-Dislocation density and *ε*-Deformation of characteristic of peaks 110 and 220 for of FAPbI₃/MAPbI₃.
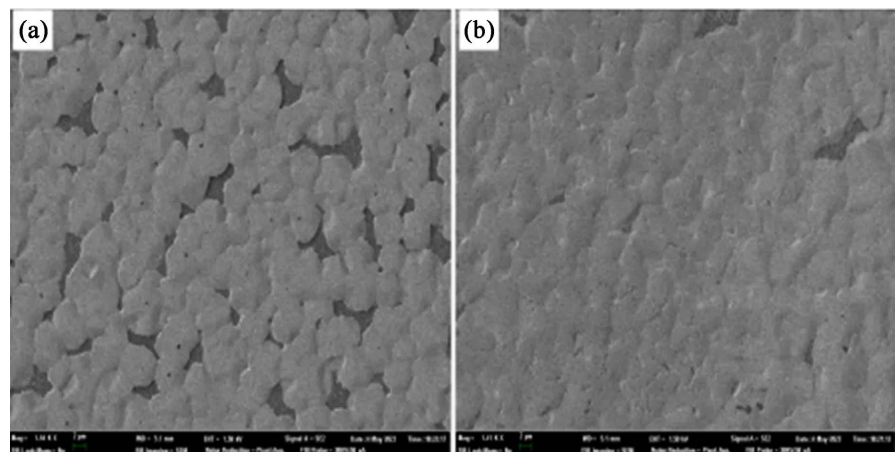
Figure 5. SEM images of FAPbI₃ and MAPbI₃ Perovskites films.

the wavelength range of 400 to 900 nm. The absorbance, transmission, and energy curves are shown in **Figure 6** & **Figure 7**. The films exhibit strong absorption in the near-infrared-visible region. Additionally, a significant increase in film absorption is observed across the entire 400 - 900 nm range, likely due to an abundance of electronic transitions at vibrational or rotational energy levels available in the absorbing materials [33]. However, a noticeable elevation of the
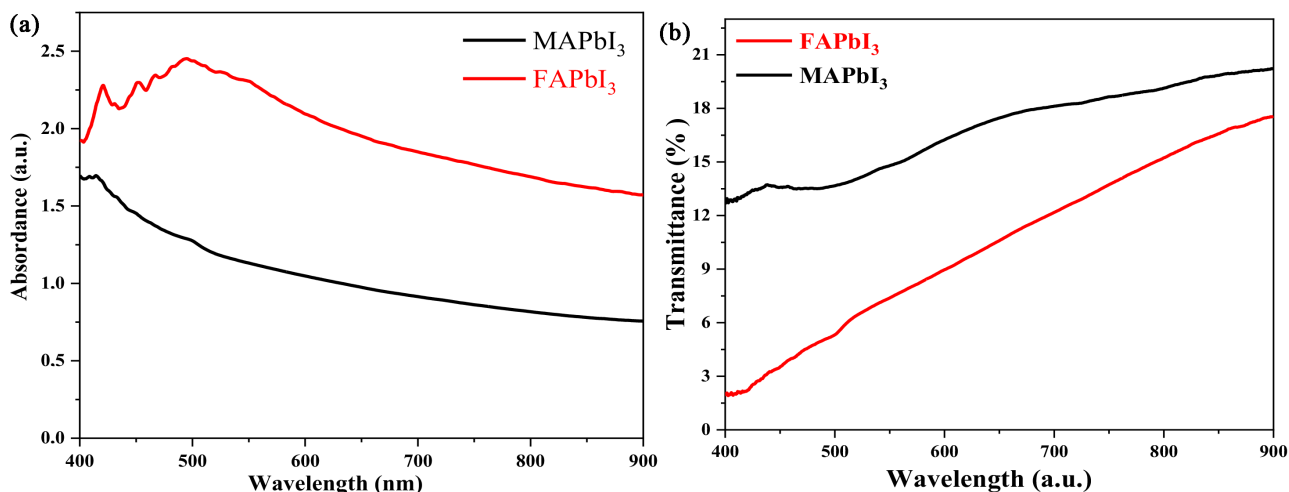
Figure 6. (a) Spectres d'absorption de FAPbI₃ et MAPbI₃ Pérovskites; (b) Spectres de transmission de FAPbI₃ et MAPbI₃ Pérovskites.
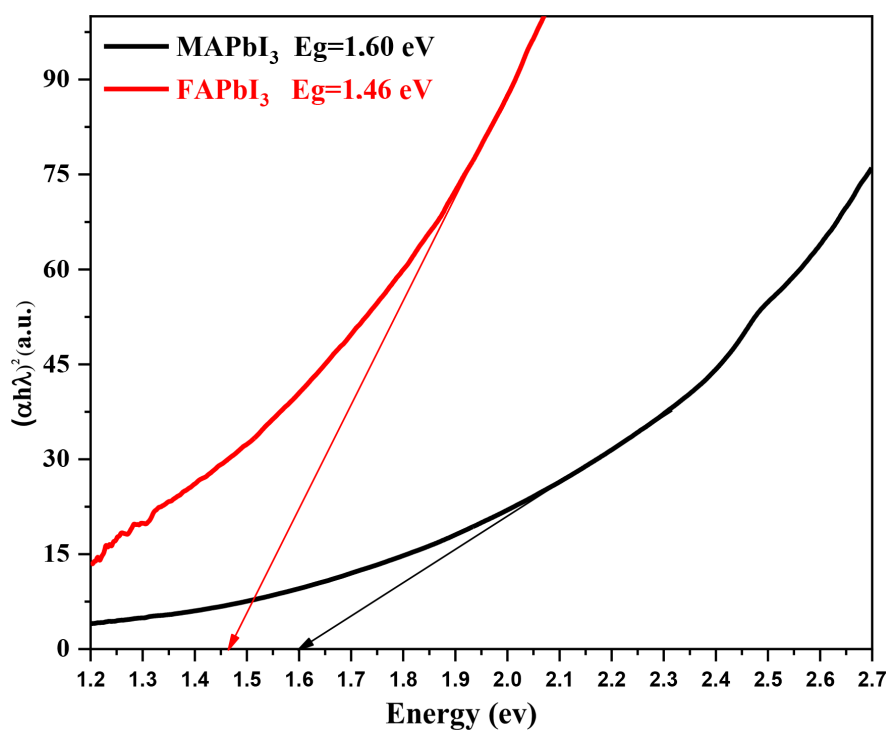
Figure 7. Band gap of FAPbI₃ and MAPbI₃ perovskites.

absorption edges in FAPbI₃ compared to MAPbI₃ is observed, with a maximum value of 2.5 (a.u.). The increased absorption in the samples can be attributed to improved crystallinity and film roughness [34]. Transmission curves have also been plotted, with the lowest value for MAPbI₃ at around 13% and the lowest transmission for the FAPbI₃ film reaching a minimum of 2%. This is in line with the XRD and SEM analyses. The film's rigidity optimizes the trapping of incident light [35].

The energy curves of the perovskites display the optical band gaps of FAPbI₃

and MAPbI₃. The band gap of FAPbI₃ is significantly lower than that of MAPbI₃. This difference could be attributed to the larger grain size of FAPbI₃ compared to MAPbI₃ [36]. The disparity in the band gaps of the films reflects a difference in lattice parameters [37].

The photoluminescence measurement spectrum allows determining the band gaps of perovskite films, which can then be compared to the band gaps obtained from energy spectra.

Figure 8 shows the photoluminescence (PL) emission spectra of FAPbI₃ and MAPbI₃ films. The FAPbI₃ film exhibits the highest photoluminescence intensity, indicating strong emission. On the other hand, the MAPbI₃ film shows weak PL emission and appears darker. The reduced PL emission of MAPbI₃ can be attributed to a lower density of surface trap states, resulting in a decrease in non radiative recombination pathways [38] [39]. This suggests that recombination predominantly occurs through radiative processes [40]. The observed PL spectra are consistent with the XRD and SEM results.

Table 3 summarizes the values of optical band gap (*Eg*) of FAPbI₃ and MAPbI₃, extracted from UV and PL measurements. A small difference is observed

Figure 8. Photoluminescence measurements of FAPbI₃ and MAPbI₃ perovskites yield band gap information, determined from peaks in the PL emission spectra.
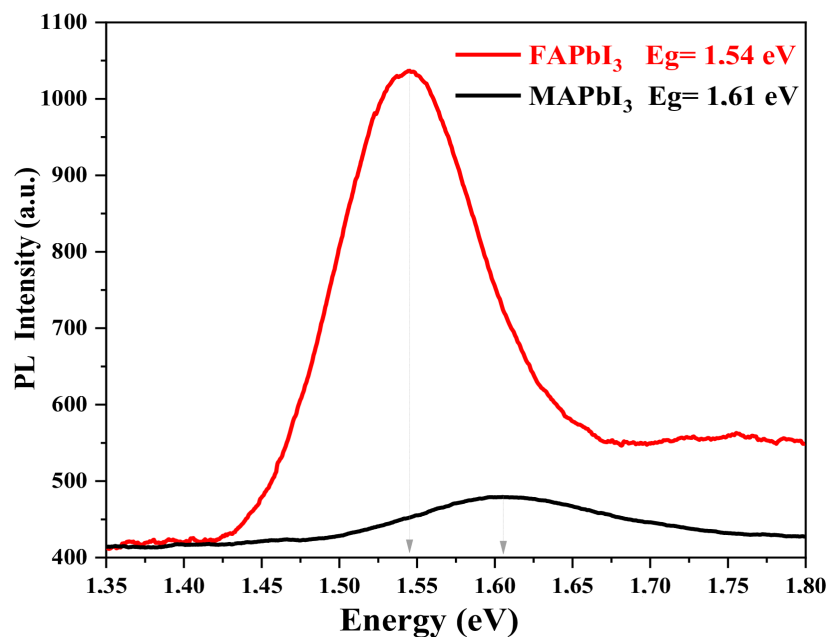
Table 3. Calculated band gaps from PL and UV-Visible measurements of FAPbI₃ and MAPbI₃ perovskites.

	MAPbI₃	FAPbI₃
$(ah\nu)^2$	1.60	1.46
PL	1.61	1.54
I∆I	0.01	0.08

between these values. The *Eg* values for FAPbI$_3$ are 1.46 eV (UV) and 1.54 eV (PL), while those for MAPbI$_3$ are 1.60 eV (UV) and 1.61 eV (PL).

The electrical resistivity of the films was measured using the four-point probe method based on the Hall effect [41]. To determine the resistivity of the perovskites, deposits were made by spin coating on simple glass substrates without FTO. Thicknesses on the order of 500 nm were found. The electrical resistivity ρ is obtained by applying the equation: $\rho = Rs \times t$, where t is the thickness and Rs is the resistivity of the thin film. $Rs = 4.5324 \times V/I$ represents the surface resistance of the film, and 4.532 is the correction factor (Figure 9).

The resistance of perovskites is measured using a low current intensity, in the nano-volt range, to avoid any alteration of the film structure due to prolonged exposure to the electrodes [42]. The films exhibit high resistivity values, primarily due to their organic nature, for both FAPbI$_3$ and MAPbI$_3$ [43] [44]. The lowest resistivity is observed for FAPbI$_3$. The resistivity and conductivity values of the charge carriers are listed in Table 4. The resistivities are very close, as are the conductivities. To facilitate the comparison of resistivities, their values have been reduced by 224, and the conductivity values have also been reduced by 438.

4. Degradation Study

The images of the aged films are obtained using the scanning electron microscopy

Table 4. Values of resistivity and conductivity for FAPbI$_3$ and MAPbI$_3$ perovskites.

sample	Je/Je (10^6 virginie)	Rs (Ω/carré)	ρ Resistivity (Ω·cm)	Conductivity (10^{-5} 1/Ω·cm)
MAPbI$_3$	1.0056	4.557	227.89	438.81
FAPbI$_3$	0.9900	4.487	224.35	445.72
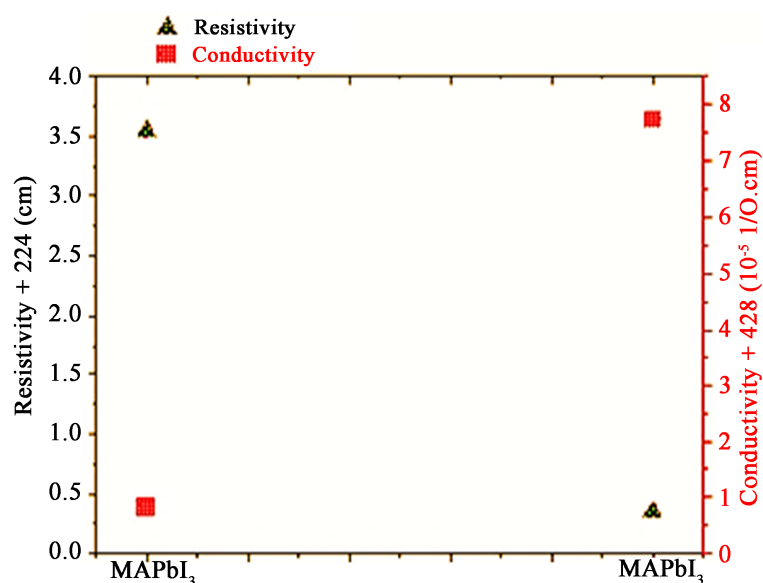
Figure 9. Resistivity and Conductivity values of FAPbI$_3$ and MAPbI$_3$ perovskites.

(SEM) technique and are presented in **Figure 10**. The degradation process has highlighted the presence of multiple pinholes as well as significant alterations in the surface morphology of the films. The image corresponding to the most deteriorated sample pertains to the MAPbI$_3$ that has been exposed to two weeks of aging in a humid environment. These findings are in line with the results obtained through X-ray diffraction (XRD) and absorption. Thus, they confirm the higher intrinsic stability of the FAPbI$_3$ film compared to the MAPbI$_3$ film [45].

The degradation mechanism of the films has undergone analysis through photoluminescence (PL) for the two aged samples presented in **Figure 11(a)** & **Figure 11(b)**. The films underwent a degradation process, and aging had a direct impact on the amplitude of the PL curves [46]. The collective PL curves of the aged films revealed a reduction in their intensity. However, it is noteworthy that the degradation curve associated with FAPbI$_3$ exhibited a less pronounced decrease compared to that of MAPbI$_3$, which lost its photoluminescence properties
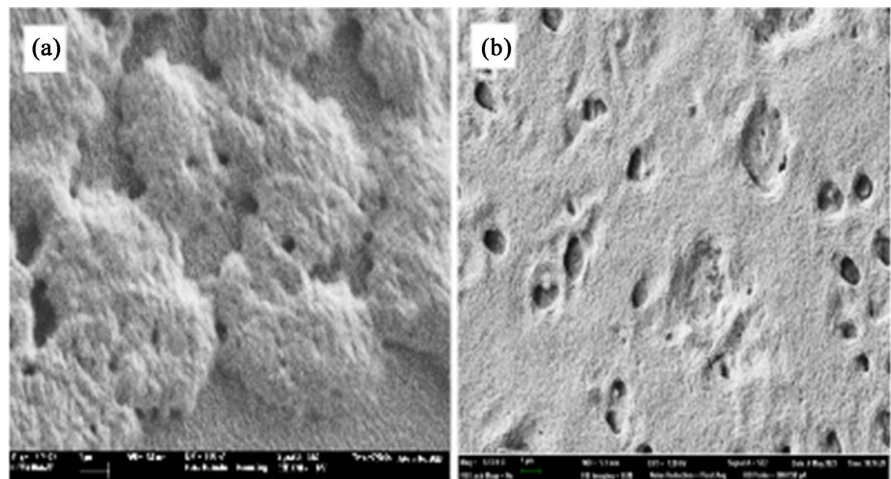
Figure 10. SEM images of two-week-aged FAPbI$_3$ and MAPbI$_3$ perovskite films.
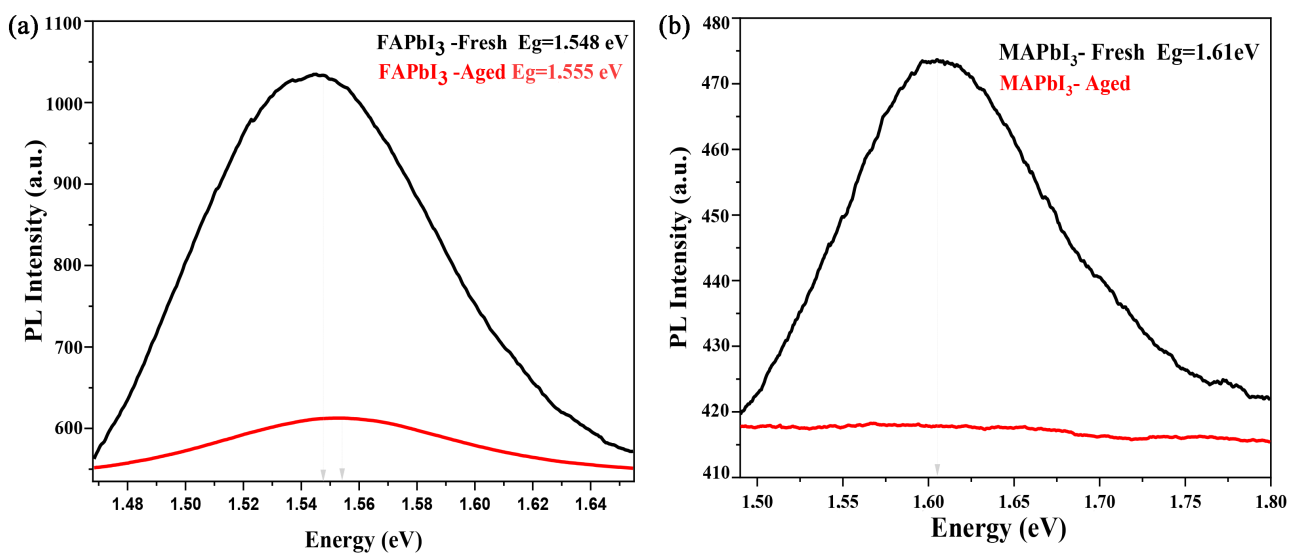
Figure 11. PL curves of fresh and aged FAPbI$_3$ and MAPbI$_3$ perovskite films.

[48] [49] [50] [51]. Additionally, a shift in the bandgap of FAPbI$_3$ was observed, transitioning from 1.548 eV for the initial sample to 1.556 eV for the degraded sample. The results from the PL measurements of the aged films align with absorption assessments, which also indicated a considerable decrease in absorption amplitudes.

Figure 12 shows the absorption spectra of both fresh and aged perovskite films. These absorption spectra reveal a difference between the films before and after aging. A decrease in absorption can be observed in all aged samples. The aged film of FAPbI$_3$ exhibits the highest absorption compared to the aged film of MAPbI$_3$.

The degradation rate curves of the films are also depicted in Figure 13. These curves illustrate the degradation speed of each film [47]. It is observed that the
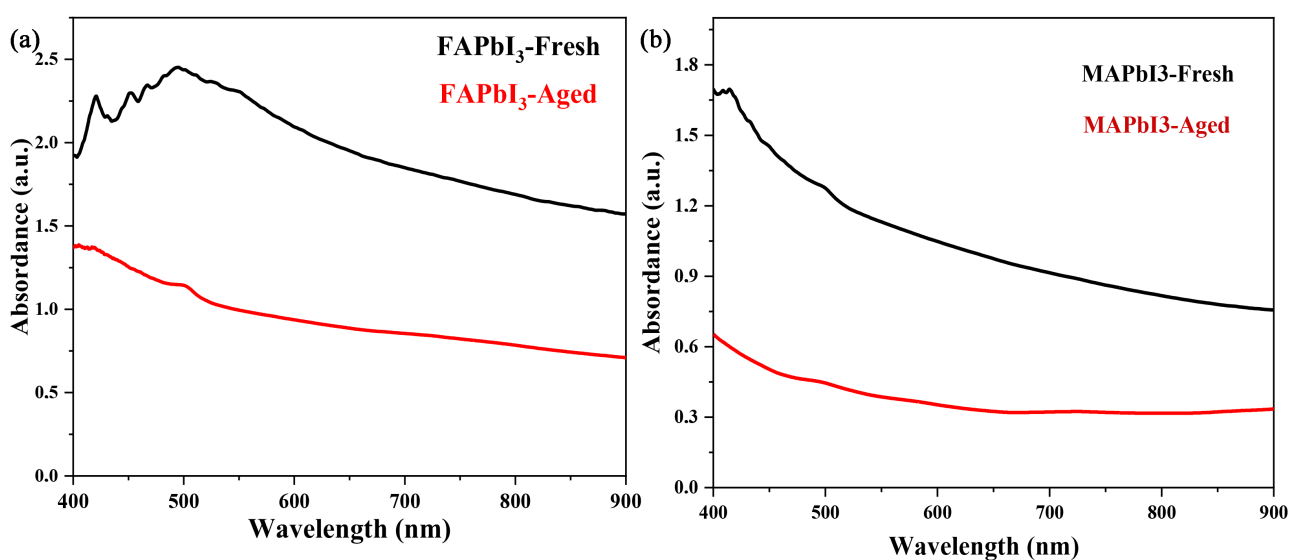
Figure 12. Absorbance spectra of fresh and aged FAPbI$_3$ and MAPbI$_3$ perovskite films.
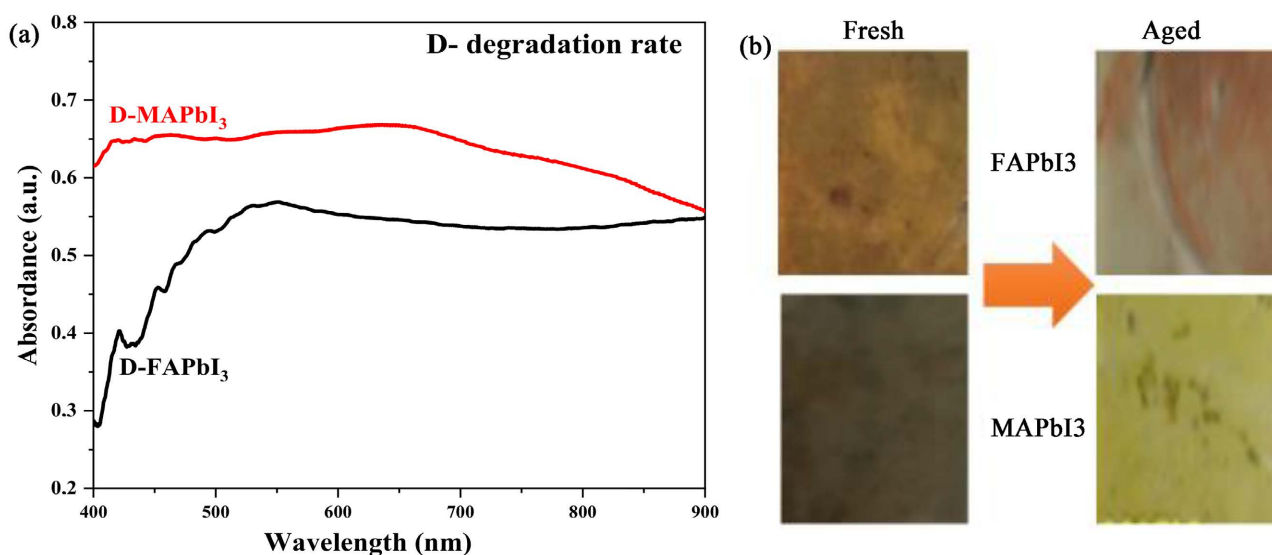
Figure 13. Photographs of fresh and aged Films and degradation rate spectra after three weeks FAPb$_x$I$_3$ MAPb$_x$I$_3$ Perovskites.

degradation curve of FAPbI$_3$ is significantly lower than that of MAPbI$_3$. The FAPbI$_3$ film undergoes degradation at a slower pace compared to the MAPbI$_3$ film, and this observation aligns with the analyses conducted through scanning electron microscopy (SEM) of the degraded films.

5. Conclusion

In this study, we analyzed the structures of FAPbI$_3$ and MAPbI$_3$ perovskites. The structural, optical, and morphological measurements have shown that the FAPbI$_3$ film exhibits improved characteristics compared to the MAPbI$_3$ film. FAPbI$_3$ demonstrates a homogeneous and rough surface, allowing for maximum trapping of incident light, unlike MAPbI$_3$. XRD results indicated the presence of residual PbI$_2$ in the MAPbI$_3$ film. SEM images revealed relatively rough surfaces for all thin films. The band gap of FAPbI$_3$ is lower than that of MAPbI$_3$, and conversely, the absorption curves of FAPbI$_3$ are significantly higher than those of MAPbI$_3$. The band gaps obtained from photoluminescence (PL) spectroscopy analysis closely match the band gaps obtained from absorption measurements. Additionally, it was observed that the FAPbI$_3$ film experiences less degradation compared to the MAPbI$_3$ film, which exhibits a yellowish coloration on the aged film, indicating the presence of the PbI$_2$ precursor. These results contribute to the fundamental understanding of the degradation mechanism of perovskites, providing strategies for designing stable and efficient perovskite-based devices.

Conflicts of Interest

The authors declare no conflicts of interest regarding the publication of this paper.

References

[1] Bouich, A. (2021) Study and Characterization of Hybrid Perovskites and Copper-Indium-Gallium Selenide Thin Films for Tandem Solar Cells. Doctoral Dissertation, Universitat Politècnica de València, Valencia.

[2] Mohammed, M.H. (2020) Etude des propriétés Structurales, Optoélectroniques et Thermodynamiques des matériaux Pérovskites et Doubles Pérovskites à base d'halogènes. Master's Thesis, Université de Mascara, Mascara.

[3] Berry, F. (2020) Nanostructuration et cristaux photoniques à base de pérovskites hybrides pour applications photovoltaïques. Master's Thesis, Université de Lyon, Lyon.

[4] Lincot, D. (2018) Où en est la conversion photovoltaïque de l'énergie solaire? *Photoniques*, **93**, 37-43. https://doi.org/10.1051/photon/20189337

[5] Bouri, N., Talbi, A., Khaaissa, Y., Derbali, S., Bouich, A. and Nouneh, K. (2022) Insight into MAPb$_{1-x}$Eu$_x$I$_3$ Based Perovskite Solar Cell Performance Using SCAPS Simulator. *Optik*, **271**, Article ID: 170235. https://doi.org/10.1016/j.ijleo.2022.170235

[6] Musy, M. and Estival, L. (2017) Vivons la ville autrement: Des villes durables où il fait bon vivre au quotidien. Editions Quae, Versailles.

[7] Bekkouche, A., Hezili, M. and Kouras, S.E. (2022) Synthèse, Caractérisation et Propriétés Photocatalytiques de quelques Oxydes Mixtes de type Pérovskite. Master's

Thesis, Université de Jijel, Jijel.

[8] Spalla, M. (2019) Stabilité intrinsèque des cellules solaires pérovskites: Impact de la formulation de la couche active et des couches de transport de charges. Master's Thesis, Université Grenoble Alpes, Saint-Martin-d'Hères.

[9] Leblanc, A. (2019) Pérovskites Halogénées pour l'électronique. Master's Thesis, Université d'Angers, Angers.

[10] Chang, C.Y., Tsao, F.C., Pan, C.J., Chi, G.C., Wang, H.T., Chen, J.J., *et al.* (2006) Electroluminescence from ZnO Nanowire/Polymer Composite p-n Junction. *Applied Physics Letters*, **88**, Article ID: 173503. https://doi.org/10.1063/1.2198480

[11] Nguyen, T.P. (2020) Introduction à l'électronique organique. Vol. 2: Applications et commercialisation. ISTE Group, London.

[12] Petibon, S. (2009) Nouvelles architectures distribuées de gestion et conversion de l'énergie pour les applications photovoltaïques. Master's Thesis, Université Paul Sabatier-Toulouse III, Toulouse.

[13] Elbaz, A. (2019) Sources laser compatibles silicium à base de Ge et GeSn à bande interdite directe. Master's Thesis, Université Paris-Saclay, Gif-sur-Yvette.

[14] Diab, H. (2017) Propriétés optiques des pérovskites hybrides 3D pour le photovoltaique. Master's Thesis, Université Paris-Saclay, Gif-sur-Yvette.

[15] Bouazizi, S., Tlili, W., Bouich, A., Soucase, B.M. and Omri, A. (2022) Design and Efficiency Enhancement of FTO/PC$_{60}$BM/CsSn$_{0.5}$Ge$_{0.5}$I$_3$/Spiro-OMeTAD/Au Perovskite Solar Cell Utilizing SCAPS-1D Simulator. *Materials Research Express*, **9**, Article ID: 096402. https://doi.org/10.1088/2053-1591/ac8d52

[16] Jemli, K. (2016) Synthése et auto-assemblage de molécules de pérovskite pour la photonique et le marquage. Master's Thesis, Université Paris-Saclay, Gif-sur-Yvette.

[17] Banouh, T. and Aoun, D. (2018) Elaboration des couches minces par le procédé Sol-Gel type Spin Coating. Master's Thesis, Université Akli Mouhand Oulhadj-Bouira, Bouira.

[18] Breniaux, E. (2021) Elaboration et caractérisation de films minces de pérovskites halogénées inorganiques: Stabilisation de dispositifs photovoltaïques par ajout de la phase 2D Cs2PbCl2I2. Master's Thesis, Université Paul Sabatier-Toulouse III, Toulouse.

[19] De Wolf, S., Holovsky, J., Moon, S.-J., Löper, P., Niesen, B., Ledinsky, M., Haug, F.-J., Yum, J.-H. and Ballif, C. (2014) Organometallic Halide Perovskites: Sharp Optical Absorption Edge and Its Relation to Photovoltaic Performance. *The Journal of Physical Chemistry Letters*, **5**, 1035-1039. https://doi.org/10.1021/jz500279b

[20] Sato, T., Takagi, S., Deledda, S., Hauback, B.C. and Orimo, S.I. (2016) Extending the Applicability of the Goldschmidt Tolerance Factor to Arbitrary Ionic Compounds. *Scientific Reports*, **6**, Article No. 23592. https://doi.org/10.1038/srep23592

[21] Pauling, L. (1931) The Nature of the Chemical Bond. Application of Results Obtained from the Quantum Mechanics and from a Theory of Paramagnetic Susceptibility to the Structure of Molecules. *Journal of the American Chemical Society*, **53**, 1367-1400. https://doi.org/10.1021/ja01355a027

[22] Kieslich, G., Sun, S. and Cheetham, A.K. (2014) Solid-State Principles Applied to Organic-Inorganic Perovskites: New Tricks for an Old Dog. *Chemical Science*, **5**, 4712-4715. https://doi.org/10.1039/C4SC02211D

[23] Shannon, R.D. (1976) Revised Effective Ionic Radii and Systematic Studies of Interatomic Distances in Halides and Chalcogenides. *Acta Crystallographica*, **A32**, 751-767. https://doi.org/10.1107/S0567739476001551

[24] Li, C., Lu, X., Ding, W., Feng, L., Gao, Y. and Guo, Z. (2008) Formability of ABX₃ (X = F, Cl, Br, I) Halide Perovskites. *Acta Crystallographica*, **B64**, 702-707. https://doi.org/10.1107/S0108768108032734

[25] Slimani, M.A. (2019) Cellules solaires pérovskites imprimées et optimisation des couches pérovskites pour les cellules tandems. Master's Thesis, École de technologie supérieure.

[26] Benkedidah, H., Kaibache, A. and Boucheloukh, H.E. (2022) Dégradation photocatalytique du bleu de méthylène et du rouge de méthyle en solution aqueuse en utilisant des oxydes mixtes. Master's Thesis, Université de Jijel, Jijel.

[27] Dally, P. (2019) Cellules Solaires à base de Matériaux Pérovskites: De la caractérisation des matériaux à l'amélioration des rendements et de la stabilité. Master's Thesis, Université Grenoble Alpes, Saint-Martin-d'Hères.

[28] Koné, K.E., Bouich, A., Marí-Guaita, J., Soucase, B.M. and Soro, D. (2023) Insight into the Effect of Halogen X in Methylammonium Lead Halide (MAPbX₃) Spin-Coated on Zinc Oxide Film. *Optical Materials*, **135**, Article ID: 113238. https://doi.org/10.1016/j.optmat.2022.113238

[29] Zhang, Y., Kim, S.G., Lee, D., Shin, H. and Park, N.G. (2019) Bifacial Stamping for High Efficiency Perovskite Solar Cells. *Energy & Environmental Science*, **12**, 308-321. https://doi.org/10.1039/C8EE02730G

[30] Al Katrib, M. (2022) Cellules solaires pérovskites réalisées par électrodéposition. Master's Thesis, Université Grenoble Alpes, Saint-Martin-d'Hères.

[31] Doumbia, Y., Bouich, A., Soro, D. and Soucase, B.M. (2022) Mixed Halide Head Perovskites Thin Films: Stability and Growth Investigation. *Optik*, **261**, Article ID: 169222. https://doi.org/10.1016/j.ijleo.2022.169222

[32] Hadjadj, A. and Chaieb, A. (2017) Synthèse de nanoparticules de ZnS et études de leurs propriétés structurales et optiques.

[33] Steveler, É. (2012) Etude des mécanismes de photoluminescence dans les nitrures et oxydes de silicium dopés aux terres rares (Er, Nd). Master's Thesis, Université de Lorraine, Lorraine.

[34] Nabila, B. (2019) Elaboration et caractérisation des couches d'oxyde de molybdène. Master's Thesis, Faculté des Sciences et Technologies, Vandœuvre-lès-Nancy.

[35] Hadjlarbi, K. (2021) Etude comparative d'une méthode d'électrodéposition directe et pulsée de films de TiO₂ et son effet sur la dégradation photoélectrocatalytique du méthylorange (MO). Master's Thesis, Université Ferhat Abbas, Setif.

[36] Touré, A., Bouich, A., Doumbia, Y., Soucasse, B.M. and Soro, D. (2023) Investigation of the Optoelectronic and Structural Properties of FA$_{(1-x)}$Bi$_x$PbBr$_6$I$_3$ of Perovskite Mixed Halide Films. *Optik*, **288**, Article ID: 171160. https://doi.org/10.1016/j.ijleo.2023.171160

[37] Fradi, K., Bouich, A., Slimi, B. and Chtourou, R. (2022) Towards Improving the Optoelectronics Properties of MAPbI$_{3(1-x)}$B$_{3x}$/ZnO Heterojunction by Bromine Doping. *Optik*, **249**, Article ID: 168283.

[38] Chehade, G. (2022) Dynamique de recombinaison et propriétés excitoniques dans les pérovskites hybrides 2D. Master's Thesis, Université Paris-Saclay, Bures-sur-Yvette.

[39] Lemercier, T. (2020) Développement de cellules solaires pérovskites semi-transparentes de type PIN dans la perspective d'une application tandem. Master's Thesis, Université Savoie Mont Blanc, Chambéry.

[40] Gayot, F. (2022) Etude de l'influence d'une intégration par ALD d'une couche

sélective d'électrons en SnO_2 dans les cellules photovoltaïques à base de pérovskite. Master's Thesis, Université Grenoble Alpes, Saint-Martin-d'Hères.

[41] Boniface, C. (2006) Modélisation et diagnostic d'un propulseur à effet Hall pour satellites: Configuration magnétique et nouveaux concepts. Master's Thesis, Université Paul Sabatier-Toulouse III, Toulouse.

[42] Daufin, G. and Talbot, J. (1971) Etude de quelques problèmes de corrosion dans l'industrie laitière. Premiere partie. Géneralités sur la corrosion des métaux et alliages. *Le Lait*, **51**, 375-398. https://doi.org/10.1051/lait:197150719

[43] Baussens, O. (2021) Nouveau matériau pérovskite pour la radiographie médicale. Master's Thesis, Université de Bordeaux, Bordeaux.

[44] Amelot, D. (2021) Etudes des propriétés d'interfaces pour les cellules solaires de nouvelle génération. Master's Thesis, Sorbonne Université, Paris.

[45] Xing, G., Mathews, N., Sun, S., Lim, S.S., Lam, Y.M., Grätzel, M. and Sum, T.C. (2013) Long-Range Balanced Electron- and Hole-Transport Lengths in Organic-Inorganic $CH_3NH_3PbI_3$. *Science*, **342**, 344-347. https://doi.org/10.1126/science.1243167

[46] Loncle, A. (2022) Nano-imageries synchrotron (Fluorescence X, diffraction X et photoluminescence) appliquées à l'étude du lien entre structure/propriété à l'échelle nanométrique dans les pérovskites hybrides pour le photovoltaïque. Master's Thesis, Université Paris-Saclay, Gif-sur-Yvette.

[47] Koné, K.E., Bouich, A., Soro, D. and Soucase, B.M. (2023) Surface Engineering of Zinc Oxide Thin as an Electron Transport Layer for Perovskite Solar Cells. *Optical and Quantum Electronics*, **55**, 1-11. https://doi.org/10.1007/s11082-023-04671-6

[48] Bouich, A., Marí-Guaita, J., Soucase, B.M. and Palacios, P. (2023) Bright Future by Enhancing the Stability of Methylammonium Lead Triiodide Perovskites Thin Films through Rb, Cs and Li as Dopants. *Materials Research Bulletin*, **163**, Article ID: 112213. https://doi.org/10.1016/j.materresbull.2023.112213

[49] Bouich, A., Torres, J.C., Chfii, H., Marí-Guaita, J., Khattak, Y.H., Baig, F., Palacios, P., *et al.* (2023) Delafossite as Hole Transport Layer a New Pathway for Efficient Perovskite-Based Solar Sells: Insight from Experimental, DFT and Numerical Analysis. *Solar Energy*, **250**, 18-32. https://doi.org/10.1016/j.solener.2022.12.022

[50] Aka, A.H., Bouich, A., Diomandé, I., Aka, B. and Soucase, B.M. (2023) Comparative Study between CZTS and CZTSe Thin Layers for Photovoltaic Applications. *E3S Web of Conferences*, **412**, Article No. 01100. https://doi.org/10.1051/e3sconf/202341201100

[51] Bouich, A., Torres, J.C., Khattak, Y.H., Baig, F., Marí-Guaita, J., Soucase, B.M., Palacios, P., *et al.* (2023) Bright Future by Controlling α/δ Phase Junction of Formamidinium Lead Iodide Doped by Imidazolium for Solar Cells: Insight from Experimental, DFT Calculations and SCAPS Simulation. *Surfaces and Interfaces*, **40**, Article ID: 103159. https://doi.org/10.1016/j.surfin.2023.103159
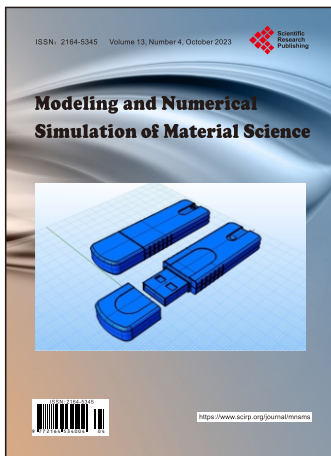
Modeling and Numerical Simulation of Material Science

Modeling and Numerical Simulation of Material Science (**MNSMS**) is an international peer-reviewed, open access journal publishing in English original research studies, reviews and case reports in all aspects of Material Science.

Honorary Editor-in-Chief

Prof. Kiet Tieu   University of Wollongong, Australia

Executive Editor-in-Chief

Prof. Hailiang Yu   Central South University, China

Subject Coverage

All the manuscripts must be prepared in English, and are subject to a rigorous and fair peer-review process. Accepted papers will immediately appear online followed by printed hard copies. The journal publishes original papers including but not limited to the following fields:

- Application of Modeling and Numerical Simulation Methods
- Artificial Intelligence Method
- Biomaterials
- Boundary Element Method
- Carbons
- Cellular Automaton (CA)
- Ceramic Materials
- Composites
- Crystal Plasticity Finite Element Method
- Ferrous Metals and Alloys
- Finite Difference Method
- Finite Element Method
- Molecular Dynamics (MD)
- Non-Ferrous Metals and Alloys
- Polymer
- Slab Method
- Statistical Methods
- Other Advanced Materials

Notes for Intending Authors

Submitted papers should not have been previously published nor be currently under consideration for publication elsewhere. Paper submission will be handled electronically through the website. All papers are refereed through a peer review process. For more details about the submissions, please access the website.

Website and E-Mail

https://www.scirp.org/journal/mnsms   E-mail: mnsms@scirp.org

What is SCIRP?

Scientific Research Publishing (SCIRP) is one of the largest Open Access journal publishers. It is currently publishing more than 200 open access, online, peer-reviewed journals covering a wide range of academic disciplines. SCIRP serves the worldwide academic communities and contributes to the progress and application of science with its publication.

What is Open Access?

All original research papers published by SCIRP are made freely and permanently accessible online immediately upon publication. To be able to provide open access journals, SCIRP defrays operation costs from authors and subscription charges only for its printed version. Open access publishing allows an immediate, worldwide, barrier-free, open access to the full text of research papers, which is in the best interests of the scientific community.

- High visibility for maximum global exposure with open access publishing model
- Rigorous peer review of research papers
- Prompt faster publication with less cost
- Guaranteed targeted, multidisciplinary audience